Nuclear Instruments and Methods in Physics Research B 554 (2024) 165452

Contents lists available at ScienceDirect

Nuclear Inst. and Methods in Physics Research, B

journal homepage: www.elsevier.com/locate/nimb

Mechanism of electrical performance degradation of 4H-SiC junction barrier Schottky diodes induced by neutron irradiation

Hao Li [a], Jingying Wang [a], Binghua Song [a], Heyi Li [b], Long Geng [c], Binghuang Duan [b,*], Shuo Zhang [a,*]

[a] School of Nuclear Science and Technology, Lanzhou University, Lanzhou 730000, PR China
[b] Institute of Electronic Engineering, China Academy of Engineering Physics, Mianyang 621900, PR China
[c] The 404 Company Limited, China National Nuclear Corporation, China

ARTICLE INFO

Keywords:
4H-SiC JBS
Acceptor traps
Neutrons irradiation

ABSTRACT

4H-SiC junction barrier Schottky diodes (JBS) were irradiated by reactor neutrons. The degradation in the electrical performance of JBS is characterized by I-V and C-V measurement, and the concentrations of traps introduced by irradiation were measured by deep-level transient spectroscopy (DLTS). TCAD simulations were employed to fit the I-V characteristics through adjusting the Schottky barrier height, concentrations of various traps induced by irradiation and the carrier mobility. The experimental results indicate that neutron irradiation would lead to an increase of the forward on-state resistance and reverse breakdown voltage. The simulation results indicates that the increase in forward on-state resistance and reverse breakdown voltage is primarily attributed to carrier capture by acceptor traps. A comparison between trap concentrations obtained from simulations and DLTS highlighted that when neutron fluence exceeds 2×10^{13} cm^{-2}, certain deep-level traps might not be entirely discernible through DLTS, particularly given a maximum measurement temperature of 500 K.

1. Introduction

SiC has exhibited outstanding performance in high-temperature, high-radiation environments, owing to its exceptional features such as high thermal conductivity, wide bandgap, elevated critical displacement energy [1], and robust breakdown field strength. The 4H-SiC Junction Barrier Schottky (JBS) diode combines the advantageous forward characteristics of low turn-on voltage and rapid switching speed from 4H-SiC Schottky Barrier Diodes (SBD), along with the favorable low reverse leakage current properties of 4H-SiC pin diodes. These features render it suitable for particle detectors [2], aerospace power switches [3] and high-energy physics experiments [4]. Consequently, studying the mechanism underlying the electrical performance degradation of 4H-SiC JBS diodes in neutron radiation fields holds substantial significance.

Over the past decade, with improvements in SiC technology based on the 4H-SiC polytype, SiC devices have gradually entered the commercial market, drawing significant attention to their radiation-induced damage. Most of the studies that explore the impact of irradiation damage on SiC JBS and PiN diodes consider these structures as SiC radiation detectors [1,2,5–7]. Only a limited number of studies have taken the JBS structure into consideration as power devices [3,8].

Irradiation by different types of particles, including electrons, protons, and neutrons, can induce similar electrical performance degradation phenomena in SiC JBS diodes, such as an increase in forward on-state resistance and a reduction in carrier concentration within the drift region [9–12]. However, the impact of irradiation varies due to the type and dosage of particles used, as well as the size and structure of the JBS device, leading to non-uniform degradation of device electrical performance following irradiation. For example, Park et al. utilized fast neutron irradiation at a fluence of 1.45×10^{13}n/cm^2 on Schottky devices with an epitaxial layer thickness of ~ 30 μm. The results revealed a decrease in the Schottky barrier height of SBD as the irradiation fluence increased [13]. However, the findings of Kleppinger et al. indicated that neutron irradiation had a minimal impact on the Schottky barrier height of SBD with an epitaxial layer thickness of 250 μm [14]. Park et al.'s study demonstrated that the leakage current of Schottky devices under a reverse bias of 70 V remained nearly unchanged after neutron irradiation at a fluence of 1.45×10^{13}n/cm^2 [13], while Liu al.'s results indicate a decrease of leakage current under low reverse bias (< ~50 V) and

* Corresponding authors.
E-mail addresses: duanbinghuang@163.com (B. Duan), zhangshuo@lzu.edu.cn (S. Zhang).

https://doi.org/10.1016/j.nimb.2024.165452
Received 26 November 2023; Received in revised form 29 May 2024; Accepted 24 June 2024
Available online 2 July 2024

a significant increase of leakage current under high reverse bias (>100 V) for SBD after neutron irradiation with a fluence of 7.29×10^{14}n/cm^2 [5]. Furthermore, there are significant variations in the reported types and concentrations of radiation-induced defects among different research groups, even for neutron-irradiated similar devices. Therefore, it is still necessary to further investigate the nature of radiation-induced defects and their impact on the electrical properties of the device.

DLTS (Deep-Level Transient Spectroscopy) is a widely utilized method for detecting radiation-induced traps in semiconductor materials. Numerous research groups have employed DLTS to measure the traps introduced by various types of particle irradiation in SiC [14–17]. The type and quantity of irradiation-induced traps strongly depend on the type of irradiating particles and the irradiation fluence. However, DLTS testing has certain limitations. For example, the heating process involved in DLTS measurements can lead to the annealing and disappearance of certain traps. In addition, certain DLTS devices may not reach the testing temperatures corresponding to specific deep-level trap peaks. For instance, in DLTS tests conducted by Park et al. [13] with a maximum temperature of 330 K and those by Capan et al. [18] with a maximum temperature of 450 K, the information about intrinsic trap EH6/EH7 was unavailable, as its peak position occurs between 500 K and 600 K. Technology Computer-Aided Design (TCAD) simulation can assist us in gaining a deeper understanding of the electrical characteristics of devices and the mechanisms behind performance degradation caused by radiation-induced traps. Thus, combining TCAD simulation with DLTS testing can provide us with more precise trap concentration information and insights into the mechanisms of device electrical performance degradation.

In this study, we intentionally induced traps in 4H-SiC JBS devices through neutron irradiation and then measured alterations in device electrical characteristics following irradiation. DLTS was utilized to determine the types and concentrations of radiation-induced traps within the devices. Subsequently, TCAD simulation was employed to model the mechanisms behind device performance degradation. The primary objective was to quantitatively elucidate the relationship between the degradation of device electrical performance and defect concentration/type through TCAD simulation and to uncover the electrical performance degradation mechanisms of JBS devices when subjected to neutron irradiation.

2. Experimental and simulation methodology

2.1. Experimental

2.1.1. Devices structure

The devices under test were 10 A/1200 V power diodes. The active region structure of these devices, as shown in Fig. 1. The device structure used in this simulation is not completely symmetrical. The rightmost p-doped zones are 0.5 μm wider than the leftmost p-doped zones. The actual device is composed of multiple cells with this structure in parallel, and the injection width of each cell is not exactly the same. Therefore, the structure of the simulated cells has a certain representativeness.

The active region is formed by the contact between the epitaxial layer and the P + region with titanium metal. The epitaxial layer is nitrogen doped with a doping concentration of 6×10^{15} cm^{-3} and a thickness of 20 μm. The anode metal is titanium metal. The contact between the anode and the P + region is an Ohmic contact, while the direct contact between the anode and the epitaxial layer is a Schottky contact, with a total contact area of 3.4 mm^2. The passivation material is SiO_2 and the packaging form is Transistor Outline Package-220 (TO-220).

2.1.2. Neutron irradiation

The diodes were irradiated with an average energy of 1 MeV neutrons at three different fluences: 1×10^{13}n/cm^2, 2×10^{13}n/cm^2, 6×10^{13}n/cm^2, utilizing the China Fast Burst Reactor-II (CFBR-II) in China

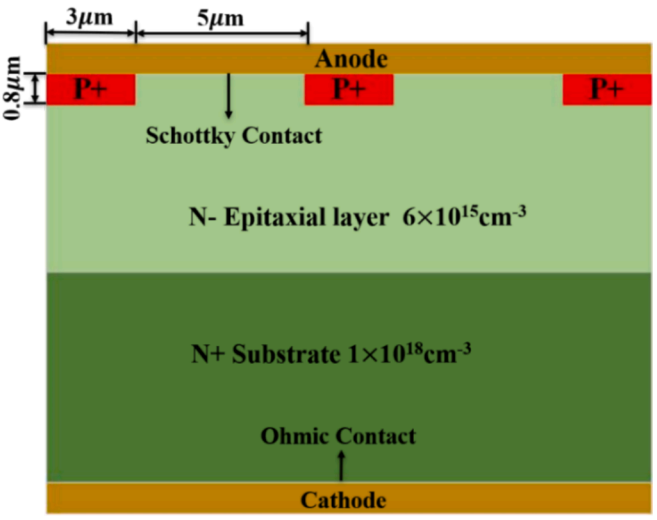

Fig. 1. Schematic of n-type 4H-SiC JBS 2D-structure.

Academy of Engineering Physics. The neutron irradiation experiments were conducted at room temperature. Corresponding to irradiation fluences of 1×10^{13}n/cm^2, 2×10^{13}n/cm^2, 6×10^{13}n/cm^2, the neutron fluence rates were 3.84×10^6 cm^{-2}·s^{-1}, 7.72×10^6 cm^{-2}·s^{-1}, and 2.30×10^7 cm^{-2}·s^{-1}, respectively. The neutron energy spectrum of CFBR-II reactor could be seen in Fig. 2 [19].

2.1.3. I-V, C-V and DLTS measurement

The electrical characteristics of the neutron-irradiated JBS devices were investigated through current–voltage (I-V) and capacitance–voltage (C-V) measurements. The I-V characteristics were recorded using a Keithley 2636-pct, while C-V characteristics were acquired with a Keithley 4200-SCS at a temperature of 300 K.

The traps were characterized using Capacitance deep-level transient spectroscopy (DLTS) with a PhysTech FT-1050. The temperature range for scanning was set from 20 to 500 K, with a reverse bias voltage (V_R) of −20 V and a pulse voltage (V_p) of −0.1 V, corresponding to the filling pulse (19.9 V) of the 4H-SiC JBS diode. The test cycle (T_w) was 19.2 ms, and the filling pulse width (t_p) was 0.1 ms, ensuring complete trap filling.

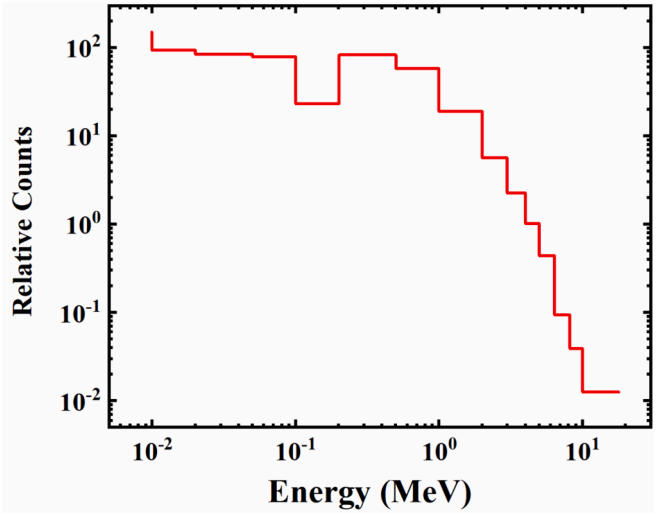

Fig. 2. The neutron spectrum of CFBR-II reactor.

2.2. Simulation methodology

TCAD simulations were performed for 4H-SiC JBS diodes, combining 4H-SiC material parameters and essential processes, such as bandgap narrowing, carrier statistics, mobility, recombination, impact ionization, and tunneling.

In the simulation of device forward characteristics, several models were introduced to account for specific processes. Due to the high ionization energy of dopants in 4H-SiC, the incomplete ionization model was introduced. The low field mobility model was based on the doping and temperature-dependent analytic model [20], while the high field mobility model utilized the parallel field-dependent Saturation Velocity Model [20]. For trap-assisted recombination, the Shockley-Read-Hall (SRH) model was applied [21,22], and a three-particle transition, where a mobile carrier is either captured or emitted, was described using the Auger recombination model [23].

In addition to the models introduced in the forward characteristics, we also incorporated the Universal Schottky Tunneling model [24,25] and Selberherr's impact ionization model [26] for simulating the reverse characteristics. It is worth noting that the Band to Band Tunneling model [27] was employed when simulating high reverse bias conditions that could lead to avalanche breakdown.

The trap model [28] were utilized to simulate the impact of traps introduced by neutron irradiation on the electrical performance of diodes. The parameters describing traps include trap energy level (E_t), trap density (n_t), as well as the electron capture cross-section (σ_n) and hole capture cross-section (σ_p) of the trap. In JBS devices, when the device operates exclusively in the Schottky forward-biased state, it is considered a unipolar device. The main current inside the device is electron conduction current. Therefore, in this context, we calibrate trap energy levels using the acceptor-like trap energy level approach, where E_t represents the trap energy level position relative to the bottom of the conduction band. We introduced the defect types obtained from our DLTS measurements and other deep-level defects reported in the literature [29], which are induced by neutron irradiation in n-type 4H-SiC, into the device structure. We assumed all traps to be non-degenerate defects, i.e., the degeneracy factors of the traps are 1. Once the trap types were identified, the trap energy levels, electron capture cross-sections, and hole capture cross-sections were determined. Since the majority of charge carriers in the devices studied in this work are electrons, the electrical characteristics are insensitive to the hole capture cross-section. Additionally, the hole capture cross-section is generally of the same order of magnitude as the electron capture cross-section. Therefore, in this work, the hole capture cross-section is set to the same value as the electron capture cross-section. which could be seen in Tab. 4. We primarily adjusted the density of different traps to fit the electrical characteristic curves of the device. It is worth noting that during the process of adjusting trap density, for double acceptor traps such as Z1/2, two electrons can be captured, and the trap concentration is only half of the concentration of capturing a single electron trap, which can achieve the same effect on I-V.

In all simulations, we maintained the device temperature at 300 K and did not consider the temperature increase caused by Joule heating in the device. The primary reason is that the main power loss in power devices is switching loss rather than conduction loss. Additionally, in the experimental tests of this work, the maximum forward voltage did not exceed 2 V, and the testing time was on the order of millisecond. These experimental conditions would not lead to an obvious change in the device temperature.

At the nanoscale, the secondary displacement defects caused by neutron elastic collisions are relatively localized. However, for the overall size of the device, due to the strong penetrating nature of neutrons, the irradiation defects inside the device can be considered as uniformly distributed. At the current level of experimental precision, it is generally considered that the damage caused by neutrons in the device is uniformly distributed. For example, Hazdra et al. tested the profiles of the dominant deep level E304 measured by DLTS in as irradiated samples and have proven that the traps are at least 4 μm uniformly distributed within the epitaxial layer [12], Consequently, in the simulation, traps were uniformly introduced into the epitaxial layer and substrate.

Taking into account the impact of radiation-induced mobility degradation, we incorporated a mobility degradation model [30], represented by eq. (1), to calculate the mobility within the epitaxial layer after irradiation.

$$\mu_n = \mu_{min} + \frac{\mu_{max} - \mu_{min}}{1 + \left(\frac{N_D}{C_r}\right)^{\alpha} + \left(\frac{N_T}{C_t}\right)^{\beta}} \tag{1}$$

N_D is the doping concentration, N_T is the total concentrations of acceptor trap, The parameter μ_{max} represents the mobility of undoped 4H-SiC, while μ_{min} is the mobility in highly doped 4H-SiC. According to reference [31], C_r, α, C_t, β are fitting parameters. $C_r = 2 \times 10^{17}\text{cm}^{-3}$, $\alpha = 0.76$, $C_t = 2.3 \times 10^{15}\text{cm}^{-3}$, $\beta = 2.9$, $\mu_{max} = 920\ \text{cm}^2/\text{V·s}$, $\mu_{min} = 10\ \text{cm}^2/\text{V·s}$.

3. Results

3.1. Forward characteristics

To investigate the impact of neutron irradiation on the performance of JBS devices, we tested the forward I-V (current–voltage) curves of the devices before and after irradiation. In Fig. 3, the black dots represent the forward characteristics of experimentally measured unirradiated samples, while the red, blue, and green dots respectively depict the forward characteristics of experimentally measured 4H-SiC JBS devices after being subjected to neutron irradiation with fluences of 1×10^{13}, 2×10^{13}, and $6 \times 10^{13}\text{n/cm}^2$. Since the forward characteristics of the device after irradiation by $1 \times 10^{13}\text{n/cm}^2$ did not show a significant change compare to the unirradiated samples, the experimental forward characters shown by the red dots in Fig. 3 almost completely overlap with the data of unirradiated samples (shown by black dots). From the Fig. 3, it can be observed that as the irradiation fluence increases, there is a noticeable decrease in the forward conduction current of the device (between about 1 to 2 V). The black, red, blue, and green solid lines in Fig. 3 represent the simulated forward characteristics of unirradiated devices and the devices irradiated with fluences of 1×10^{13}, 2×10^{13}, and $6 \times 10^{13}\text{n/cm}^2$. It can be seen from the Fig. 3 that the simulated results showed a good agreement with the experimental results. This

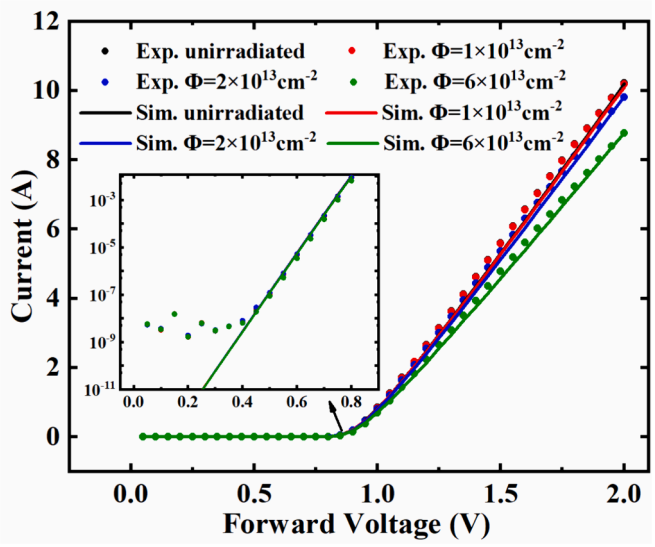

Fig. 3. Experimental and simulated forward characteristics of 4H-SiC JBS irradiated with different fluences. (Inset: Forward ln(I)-V curve).

agreement indicates that our simulation can reasonably describe the current conduction mechanism of the device.

From Fig. 3, it can be observed that the threshold voltage of the JBS device is approximately 0.8 V. The current of the device could span several orders of magnitude before conduction. To clearly illustrate the changes in current for the device at applied forward voltages below the conduction voltage, we presented the forward curves before and after irradiation using logarithmic coordinates in the 0 to 0.8 V range. The results are shown in the inset of Fig. 3. It is evident that there is almost no change in the device within the 0 to 0.8 V range before and after irradiation, as almost all experimental data overlap with the unirradiated results, and simulation results also closely match. However, there is a noticeable difference between the simulation results and experimental results in the 0 to 0.4 V range, and this difference is likely due to the fact that at very low voltage, surface currents within the device during experimental testing cannot be ignored and become a significant factor in the forward current.

The JBS devices are composed of both PN junctions and Schottky junctions. To determine the conduction region of JBS devices, we conducted TCAD simulations of the current distribution within the JBS device at a forward voltage of 2 V. The current density distribution in the present device is shown in Fig. 4. From this figure, we can conclude that the conduction mainly occurs at the Schottky junctions formed by the metal and the epitaxial layer. This conclusion is consistent with the result got by a JBS device with a similar structure [32]. Consequently, for the JBS device studied in this work, the forward conduction characteristics primarily reflect the characteristics of the Schottky junction.

The forward conduction current of the Schottky junction can be described using the theory of thermionic electron emission [33], as expressed in equation (2) and (3).

$$I_s = AA^* T^2 \exp\left[\frac{-q\varnothing_B}{kT}\right] \tag{2}$$

$$I = I_s\left[\exp\left(\frac{q(V - IR_s)}{\eta kT}\right) - 1\right] \tag{3}$$

Where I_s is the reverse saturation current, I is the current, A is the cross-sectional area of the device. A^* is Richardson constant and its value for 4H-SiC is 146 A cm^{-2} K^{-2} [34]. T is the temperature. q is the electronic charge, Φ_B is the Schottky barrier-height. K is Boltzmann's constant. V is forward bias voltage, R_s is series resistance, η is ideality factor. According to these equations, the device parameters Φ_B, η *and* R_s were extracted through fitting the experimental forward I-V curves. The results could be seen in the Table 1. From the table, we conclude that the ideality factor and Schottky barrier-height of devices were almost did not change when subjecting to the neutron irradiation within the range of fluence 6×10^{13}n/cm^2. However, series resistance showed an obvious increase with the increase of neutron fluence. Hazdra's research results [29] also indicate that within this radiation fluence range, irradiation causes almost no changes in the ideal factor and Schottky barrier height of JBS devices, while a significant increase in conduction resistance occurs.

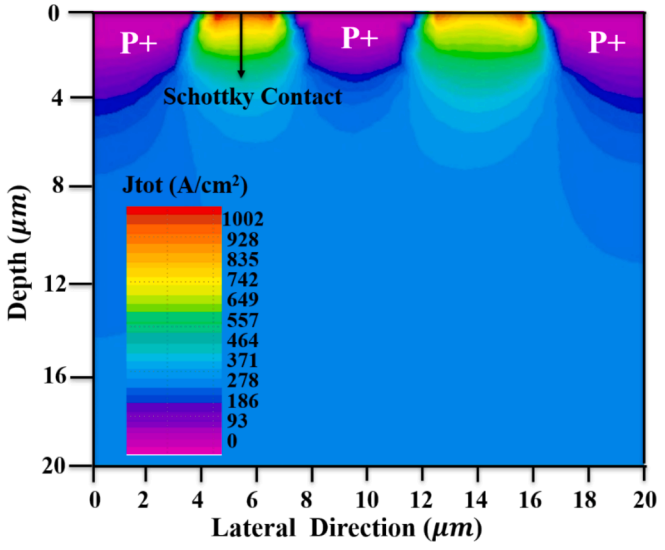

Fig. 4. Simulated 2D current density in the on state forward voltage $V_F = 2.0$ V.

To understand the reasons for changes in the performance of JBS devices due to neutron irradiation, we conducted fitting of the experimental results by adjusting the Schottky barrier height, different types of trap concentrations, and electron mobility in TCAD simulations. The simulation results in Fig. 3 show a good agreement with the experimental results. Table 2 provides the simulated Schottky barrier height, the total concentration of deep-level acceptor traps with E_t greater than 0.3 eV, and the electron mobility. From the table, it can be observed that with an increase in neutron irradiation fluence, the total concentration of deep-level acceptor traps with E_t greater than 0.3 eV increases, and the electron mobility shows a slight decrease. The increase in the concentration of deep-level acceptor traps effectively compensates for the electron concentration in the epitaxial layer, causing a reduction in the electron concentration in the epitaxial layer, the decrease in the electron concentration in the epitaxial layer is the primary reason for the increase in the device's forward series resistance. Here, in the simulation of the forward characteristics, we did not provide different types of acceptor traps concentrations but rather the total concentration of acceptor traps with E_t greater than 0.3 eV. The reason for this will be discussed in Section 4.

3.2. C-V characteristics

The experimental C-V curves of the device before and after irradiation are shown in Fig. 5. The black dots in the figure represent the C-V characteristics of the unirradiated device, while the red and blue dots respectively represent the C-V characteristics for the device irradiated with fluences of 1×10^{13} and 6×10^{13}n/cm^2. From Fig. 5, it can be observed that when the neutron irradiation fluence reaches 6×10^{13}n/cm^2, there is a noticeable decrease in the device's capacitance. According to reference [1], the relationship between the capacitance of the device and the effective carrier concentration can be expressed by equation (4).

$$\frac{1}{C^2} = \frac{2(V_{bi} + V_R)}{q\varepsilon_s\varepsilon_0 N_{eff}} \tag{4}$$

Where, C is the Capacitance, ε_s is the dielectric constant, ε_0 is the permittivity of vacuum, N_{eff} is the effective carrier concentration, V_{bi} is the built-in-potential, V_R is the reverse bias voltage. If we assume that under the irradiation fluence in this work, the dielectric constant ε_s do not change significantly due to irradiation, the square of capacitance is directly proportional to the effective carrier concentration, the extraction of effective carrier concentration is shown in Table 3. Therefore, the decrease in capacitance indicates a reduction in the effective carrier concentration within the device after 6×10^{13}n/cm^2 neutron irradiation, which is consistent with the results of the forward characteristics analysis.

Table 1
Device parameters determined from of the experimental forward I-V curves.

Sample	Φ_B (eV)	η	R_S (mΩ)
Pre-irradiation	1.23	1.01	95.60
Neutron irradiation (Φ=1 × $10^{13}$$cm^{-2}$)	1.21	1.11	95.60
Neutron irradiation (Φ=2 × $10^{13}$$cm^{-2}$)	1.22	1.06	101.20
Neutron irradiation (Φ=6 × $10^{13}$$cm^{-2}$)	1.23	1.03	114.00

Table 2
Device parameters and traps parameters used to simulate JBS irradiation with different neutron fluences.

Fluence (cm^{-2})	unirradiated	1×10^{13}	2×10^{13}	6×10^{13}
Schottky barrier height (eV)	1.23	1.23	1.23	1.23
Total concentration of acceptor traps (cm^{-3})	8×10^{13}	1.15×10^{14}	3×10^{14}	9.6×10^{14}
Electron mobility ($cm^2V^{-1}S^{-1}$)	860.73	860.65	858.63	802.02

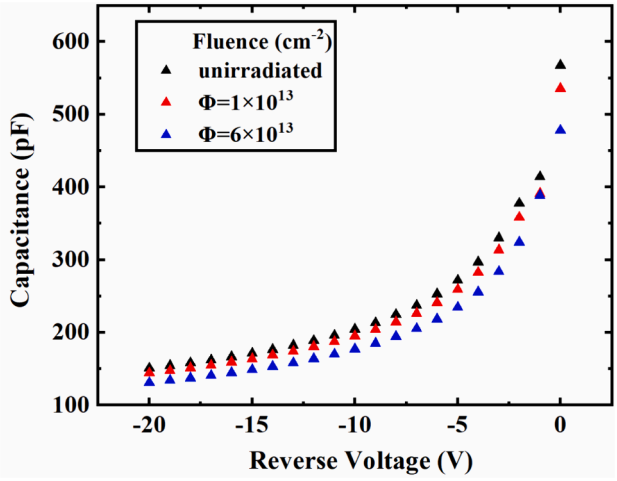

Fig. 5. Experimental C-V characteristics of 4H-SiC JBS before and after neutron irradiation.

Table 3
Effective carrier concentration determined from of the experimental C-V characteristics.

Sample	N_{eff} (cm^{-3})
Pre-irradiation	6.20×10^{15}
Neutron irradiation (Φ=$1 \times 10^{13}cm^{-2}$)	5.69×10^{15}
Neutron irradiation (Φ=$6 \times 10^{13}cm^{-2}$)	4.70×10^{15}

3.3. Reverse breakdown characteristics

The results of experimental measurements and simulations for the reverse characteristics near the breakdown voltage are shown in Fig. 6, where the solid points and lines represent the experimental and simulated results, respectively. From the experimental results, it can be observed that except for the irradiation fluence at $1 \times 10^{13}n/cm^2$, the breakdown voltage of the device increases with the increase of irradiation fluences. At the irradiation fluence of $1 \times 10^{13}n/cm^2$, since the breakdown characteristics of the device are less affected by irradiation, the impact is primarily attributed to the inherent variations of the device rather than irradiation effects. The simulation conditions for the reverse characteristics are consistent with those for the forward characteristics (specific simulation conditions can be found in Table 2). From the simulation of the reverse characteristics, we can also observe that at an irradiation fluence of $1 \times 10^{13}n/cm^2$, the breakdown voltage of the device remains nearly unchanged. However, with an increase of irradiation fluence, there is a clear trend of increasing breakdown voltage, which is consistent with the trend of reverse characteristic changes in reference [29]. From the comparison of experimental and simulated results, it can be seen that the increase in breakdown current with voltage is more gradual in the experimental results. This discrepancy

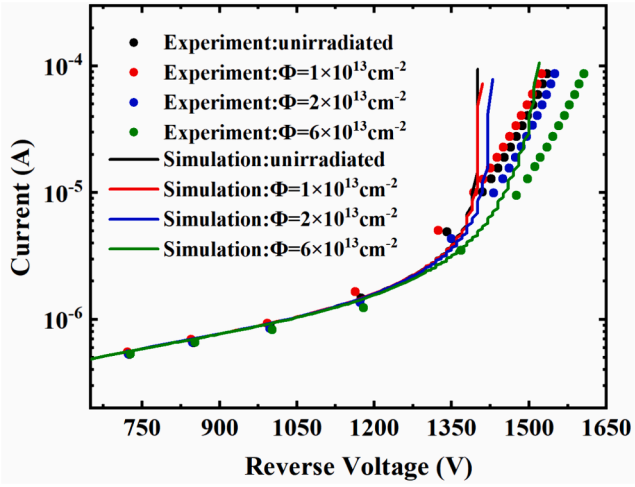

Fig. 6. Experimental and simulated reverse characteristics of devices before and after irradiation.

might be due to certain deviations between the actual device fabrication and the simulated structure. Specifically, the doping profile of the P + region in the simulation is an ideal rectangular shape, whereas in the actual device, the sharp corners of the P + region are inevitably rounded off during fabrication. This rounding of the corners can improve the breakdown characteristics, leading to a slightly slower increase in breakdown current in the experimental results. Although there are some differences between the simulation and experimental results due to non-ideal factors in device fabrication, the consistent trend between the simulation and experimental results suggests that the simulation is able to reasonably describe the real device breakdown process.

To study the reverse breakdown process of the JBS devices, we observed the electric field and total current density distribution within the unirradiated device near the breakdown voltage (1400 V) in TCAD simulations. The results are shown in Fig. 7 (a) and (b), respectively. From the electric field distribution (Fig. 7 (a)), it can be seen that the maximum electric field within the device is located in the junction region formed by P + and the epitaxial layer. Additionally, from the total current density distribution (Fig. 7 (b)), the breakdown characteristics of the device are mainly determined by the width of the p-n junction formed by the p-doped zone and epitaxial layers, it will first breakdown from the wider p-doped zones side.

To study the impact of irradiation on the device's breakdown process, we compared the electric field at the positions of the maximum electric field within the device after irradiation with different fluences. Fig. 8 compares the electric field near the breakdown position (shown in Fig. 7 (b)) of the device under different neutron irradiation fluence. From the comparison, it can be observed that at the same reverse voltage, except for the irradiation fluence of $1 \times 10^{13}n/cm^2$ where the field strength is the same as the unirradiated sample, the electric field at the breakdown positions decreases with the increase in irradiation fluence. This decrease of the electric field strength at the breakdown positions is the main reason for the increase in the breakdown voltage of the device with the increase in irradiation fluence.

3.4. DLTS result

DLTS stands as a widely adopted technique for discerning traps in both Schottky and p-n junctions, providing information on trap energy levels, concentrations, and cross-sections. As depicted in Fig. 9, DLTS spectra for intrinsic traps in the 4H-SiC JBS are presented alongside spectra for traps induced by neutron irradiation at different fluences.

In the unirradiated sample, three traps were identified, with peaks at 70 K, 165 K, and 437 K, respectively. Post neutron irradiation, six peaks

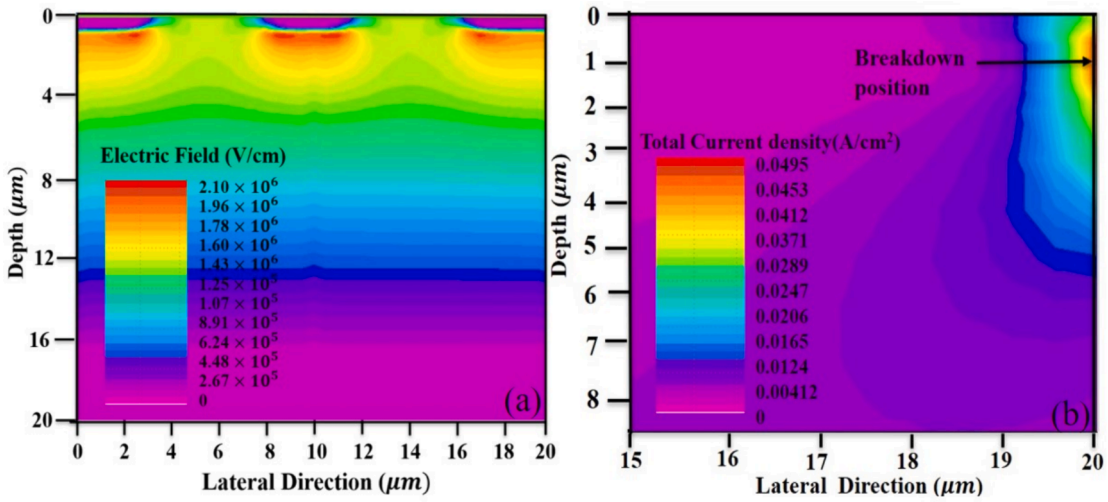

Fig. 7. (a) Simulation of electric field distribution and (b) current distribution electric in unirradiated JBS, when V_R = 1400 V.

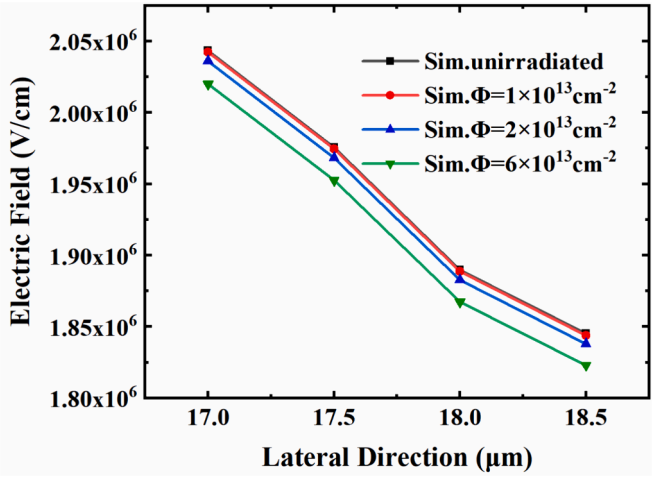

Fig. 8. Simulation of electric field distribution near the breakdown positions.

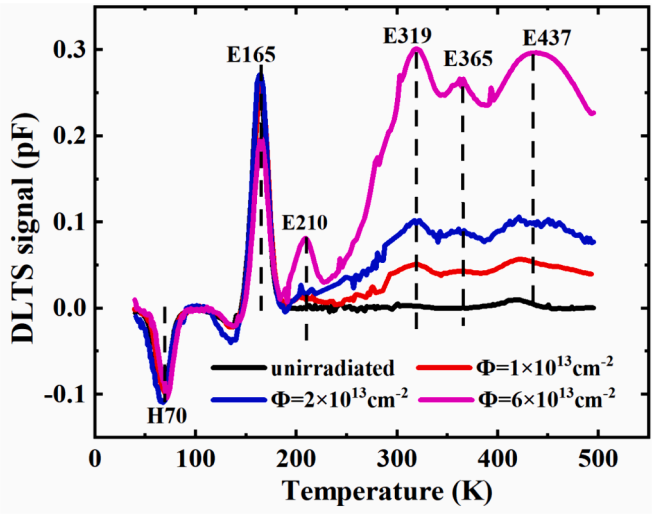

Fig. 9. DLTS spectra of 4H-SiC JBS before and after neutron irradiation.

surfaced, occurring at 70 K, 165 K, 210 K, 319 K, 365 K, and 437 K, respectively. H70 and E165 trap peaks remained consistent irrespective of neutron fluence increase, whereas E437 peaks exhibited an increasing trend with fluence increase. At a neutron fluence of 1×10^{13}n/cm^2, two new peaks E319 and E365 were detected in the sample, with subsequent increases in their respective trap peaks with increasing fluence. At a neutron fluence of 6×10^{13}n/cm^2, trap E210 appeared. Parameters for fitting each trap, based on the Arrhenius relationship [13], are detailed in Table 4.

The appearance of the E_v + 0.13 in the low-temperature region is attributed to the capture of minority carriers.[17]. The E_C-0.33 has been attributed to the carbon interstitial (C_i) [35]. The trap Ec-0.42 in this work is the same as the trap S1 reported in the literature [36], with a structure of V_{Si} (−3/−). The trap E_C-0.67 is the same as Z2 reported in the literature [37], corresponding to a trap structure of Vc (=/0). The trap Ec-0.78 is the same as the trap S2 reported in the literature [36], with a structure of V_{Si} (=/−). The trap E_C-0.995 is the same as EH4/5 reported in the literature [38], and the corresponding structure is Csi-Vc (+/0).

4. Discussion

Both TCAD simulations and DLTS measurements provided the trap concentrations within the device after irradiation at different neutron fluences. However, in TCAD simulations, we found that for JBS devices, the forward and reverse breakdown characteristics of the device are insensitive to the trap energy levels of deep-level traps (E_t > 0.3 eV). As long as the total concentration of deep-level traps is set to an appropriate value, the simulated forward and reverse breakdown characteristics could match well with experimental results. This is why in the simulation process, we only provide the total concentration of deep-level traps and do not separately present the concentration of each type of trap. To elucidate the reasons behind this result, we analyze the ionization probability of acceptor-type traps by Simmons and Taylor Theory [28]. The ionization probability of acceptor-type traps could be expressed by the following equations.

$$F_{tA} = \frac{v_n \sigma_n n + e_{pA}}{v_n \sigma_n n + e_{pA} + v_p \sigma_p p + e_{nA}} \tag{5}$$

$$e_{nA} = v_n \sigma_n n_i exp \frac{E_t - E_i}{kT_L} \tag{6}$$

$$e_{PA} = v_P \sigma_p n_i exp \frac{E_i - E_t}{kT_L} \tag{7}$$

Table 4
Identification parameters of traps detected in 4H-SiC JBS before and after neutron irradiation.

Trap label	Bandgap position(eV)	$N_t(cm^{-3})$ unirradiated	$N_t(cm^{-3})$ 1×10^{13}	$N_t(cm^{-3})$ 2×10^{13}	$N_t(cm^{-3})$ 6×10^{13}	SIGN (cm^2)
H70	$E_v + 0.13$	3.15×10^{13}	3.2×10^{13}	3.52×10^{13}	3.3×10^{13}	6.09×10^{-13}
E165	E_C-0.33	7.76×10^{13}	7.73×10^{13}	7.72×10^{13}	6.22×10^{13}	4.36×10^{-14}
E210	E_C-0.42	–	–	–	2.62×10^{13}	1.22×10^{-15}
E319	E_C-0.67	–	1.27×10^{13}	2.3×10^{13}	7.72×10^{13}	1.08×10^{-14}
E365	E_C-0.78	–	1.08×10^{13}	2.05×10^{13}	6.39×10^{13}	1.51×10^{-15}
E437	E_C-0.995	2.41×10^{12}	1.4×10^{13}	2.33×10^{13}	7.38×10^{13}	5.04×10^{-14}

Where σ_n and σ_p denote the carrier capture cross sections for electrons and holes respectively. v_n and v_p represent the thermal velocities for electrons and holes. E_i is the intrinsic Fermi level position, k is the Boltzmann constant, T_L is the lattice temperature, e_{nA} and e_{pA} are the electron and hole emission rates for acceptor traps. Based on these equations, the relationship between acceptor energy levels and the ionization probability was shown by Fig. 10. As seen from the figure, all acceptor traps tend towards complete ionization when E_t exceeds 0.3 eV, where E_t represents the trap energy level position relative to the bottom of the conduction band. Consequently, all acceptor-type traps with E_t deeper than 0.3 eV can effectively compensate for the electron concentration, leading to a decrease in the carrier concentration within the epitaxial layer. And the increase in on-state resistance and breakdown voltage is primarily caused by the decrease of carrier concentration. As a result, the changes in the performance of JBS devices in this work are insensitive to the trap energy levels of deep-level traps ($E_t > 0.3$ eV). It is worth mentioning that since the epitaxial layer of the device studied in this work is composed of n-type semiconductor, the electrical performance of the device is more sensitive to deep-level acceptor traps. Therefore, this work only reports the concentration of acceptor-type traps. However, neutron irradiation can still generate deep-level donor defects in the epitaxial layer of the device. Due to the insensitivity of the device's IV characteristics to deep-level donor defects, we are unable to study the concentration of these defects.

Comparison of trap concentration obtained from TCAD simulations and DTLS measurements is shown in Fig. 11. The black dashed line in the figure represents the trap concentration obtained from TCAD simulations, while the blue dashed line represents the trap concentration obtained from DLTS measurements. It can be seen from the figure that the trap concentration obtained from TCAD simulations was much higher than the results obtained from DLTS measurements. The reason for this discrepancy may lie in the fact that the temperature range for DLTS

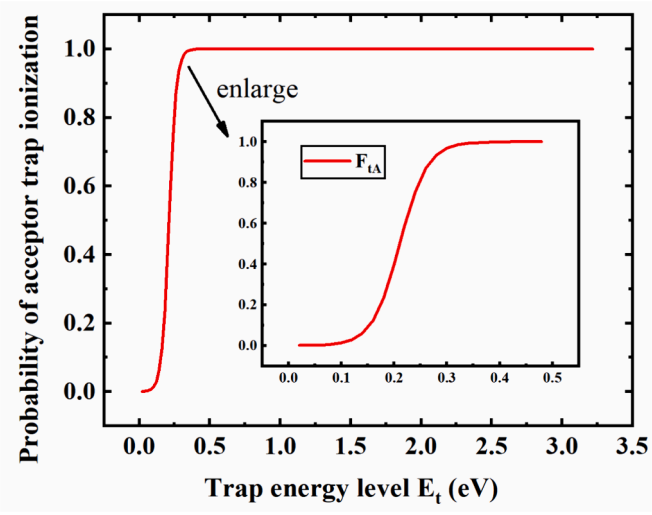

Fig. 10. The relationship between acceptor energy levels and ionization probabilities.

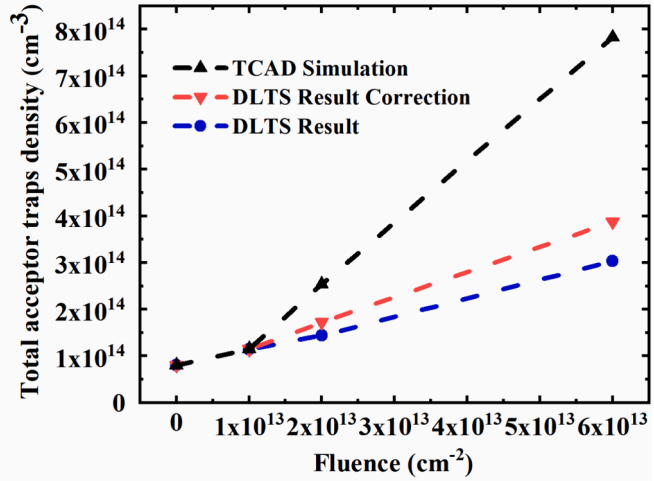

Fig. 11. Comparison of total trap concentrations obtained from TCAD Simulations and DLTS spectra.

measurements in this work were 20–500 K, and some deep-level traps have energy levels beyond this temperature range, resulting in DLTS results reflecting only a portion of the deep-level trap concentrations. This phenomenon can be verified by the DLTS test results of Hazdra et al [12]. In their studies, they utilized DLTS to investigate neutron-irradiated SiC samples over a temperature range of 20–700 K. The results indicated that some irradiation-induced traps, such as EH5, EH6/EH7 [35], exhibit energy levels beyond the 500 K temperature range. Based on the proportion of traps generated by neutrons, we corrected the trap concentration obtained from the DLTS tests in this work, as shown by the red dashed line in Fig. 11. The trap concentration in the corrected DLTS results is still lower than the trap concentration given by the simulation, indicating that at higher neutron radiation fluences, there may be traps with even deeper energy levels, beyond the DTLS testing range of 700 K, and unknown deep level traps may be able to capture multiple electrons. Nava F et al. [6] conducted DLTS testing on neutron irradiated devices, the research results indicate deep level traps such as SN5 (E_C-1.50) have higher concentrations compared to other traps, which also confirms the rationality of our inference that there are unknown deep level traps in the device.

Due to the close mass of protons and neutrons, during elastic collision processes, these two particles with the same scattering angle can generate approximately similar secondary displacement processes in the material. Therefore, at low irradiation doses, these two particles can generate some similar defects. For example, the defects with energy level of E_c-0.42 and E_c-0.68 were observed in 4H-SiC devices irradiated with both protons [17] and neutrons [12]. However, due to differences in the probability and nature of elastic collisions between protons and neutrons with material atoms, there are significant variations in the distribution and types of defects produced by the two particles, leading to distinct impacts on electrical properties. The defects generated by the proton radiation mainly extend along the incident path and reach a peak at the position of the Bragg peak, while defects generated by reactor

neutron radiation are usually uniformly distributed in materials with thickness of hundreds of μm. Vobecký et al. [11] measured the electron concentration within 3.5 μm of the epitaxial layer after proton irradiation, and found that the electron concentration had a minimum value at 2 μm, while Hazdra et al. [12] measured the concentration of E304 defects within 4 μm of the epitaxial layer after neutron irradiation and found that the defect concentration was uniformly distributed along the epitaxial layer. As protons exhibit a higher probability of elastic scattering with matter, they may produce a more concentrated distribution of cascade collision processes compared to neutrons, and there may even be an overlap of cascade collisions, leading to a more complex defect structure. Overall, while protons and neutrons share similarities in elastic scattering, their differences in interaction probability and form with mater still result in significant variations in the distribution, quantity, and types of defects they induce within the device.

There are some differences in the interactions of neutrons, protons, and electrons with device materials. Neutrons are neutral particles, and their interaction with the material occurs through secondary effects, such as elastic scattering. Protons, being relatively massive charged particles, mainly interact with 4H-SiC material through nuclear collisions and electronic energy loss. Electrons, being relatively lighter charged particles, primarily interact with the material through ionization excitation and bremsstrahlung. Therefore, there may be differences in the types of traps generated by different particle irradiation. For example, proton irradiation produces a defect $RD_{1/2}$ with an energy level of E_C-0.88 eV, which was not found in our DLTS result. Even under irradiation of different particle types, although the generated defect energy levels are the same, their corresponding damage structures may also be different. For example, both low-energy electron and fast neutron irradiation can produce defects with energy levels of E_C-0.4 eV and E_C-0.7 eV. The two defects generated by electron irradiation of 4H-SiC are called EH1/3, and the two defects generated by neutron irradiation are called S1/2, the defect EH1/3 is attributed to the different charge states of the carbon interstitial C_i, while the defect S1/2 is attributed to V_{Si} (−3/=) and V_{Si} (=/-) [39].

5. Conclusion

We investigated the electrical degradation mechanism of 4H-SiC JBS under reactor neutron (at an average energy of 1 MeV) irradiation with a maximum fluence of 6×10^{13} cm^{-2} through experiments and TCAD simulations. The simulation results are in agreement with the experimental results. The forward characteristics reveal the Schottky barrier height of the device remains nearly unchanged. The increase in device series resistance under high neutron fluence is attributed to the compensation of electron concentration in the epitaxial layer by the acceptor traps introduced by neutron irradiation, which is further confirmed by C-V characteristics. Additionally, the increase in reverse breakdown voltage is also due to the reduction in electron concentration caused by the acceptor traps introduced by irradiation, leading to a reduction in electric field strength. DLTS results reveal that the concentrations of traps H70 and E165 remain unchanged with increasing neutron irradiation fluence. In contrast, the concentrations of traps E319, E365, and E437, exhibit an increase with higher neutron irradiation fluence. A novel acceptor trap, E210, emerges at a neutron fluence of 6×10^{13} cm^{-2}. However, due to the limitation of the temperature range of DTLS measurements, the total concentration of acceptor traps obtained from DTLS was lower than that obtained from simulations. Therefore, we infer the presence of unmeasured acceptor traps in DTLS measurements for the samples subjected to neutron irradiation with fluence higher than 2×10^{13} cm^{-2}, and unknown deep level traps may be able to capture multiple electrons.

CRediT authorship contribution statement

Hao Li: Writing – review & editing, Writing – original draft, Software, Methodology, Investigation, Data curation. **Jingying Wang:** Software. **Binghua Song:** Investigation. **Heyi Li:** Methodology, Data curation. **Long Geng:** Supervision. **Binghuang Duan:** Writing – review & editing. **Shuo Zhang:** Writing – review & editing, Project administration, Investigation.

Declaration of competing interest

The authors declare that they have no known competing financial interests or personal relationships that could have appeared to influence the work reported in this paper.

Data availability

Data will be made available on request.

Acknowledgements

This work was supported by the National Natural Science Foundation of China (Grants No. 12305302 and 12005200) and the State Key Laboratory of Nuclear Physics and Technology, Peking University (funding No. NPT2023KFYI1). Grants of computer time from the Supercomputing Center of Lanzhou University, China, are gratefully acknowledged.

References

[1] S. Tripathi, C. Upadhyay, C.P. Nagaraj, A. Venkatesan, K. Devan, The performance simulation of the LiH-SiC-based Fast Neutron Detector for harsh environment monitoring using Geant4 and TCAD, Nucl. Instrum. Methods Phys. Res. A 916 (2019) 246–256.
[2] L. Liu, A. Liu, S. Bai, L. Lv, P. Jin, X. Ouyang, Radiation Resistance of Silicon Carbide Schottky Diode Detectors in D-T Fusion Neutron Detection, Sci. Rep. 7 (2017) 13376.
[3] L. Zhiyun, C. Tianbing, J.D. Cressler, D.C. Sheridan, J.R. Williams, R.A. Reed, P. W. Marshall, Impact of proton irradiation on the static and dynamic characteristics of high-voltage 4H-SiC JBS switching diodes, IEEE Trans. Nucl. Sci. 50 (2003) 1821–1826.
[4] M. Moll, Development of radiation hard sensors for very high luminosity colliders—CERN-RD50 project, Nucl. Instrum. Methods Phys. Res. A 511 (2003) 97–105.
[5] L.Y. Liu, T.L. Shen, A. Liu, T. Zhang, S. Bai, S.R. Xu, P. Jin, Y. Hao, X.P. Ouyang, Performance degradation and defect characterization of Ni/4H-SiC Schottky diode neutron detector in high fluence rate neutron irradiation, Diamond Relat. Mater. 88 (2018) 256–261.
[6] F. Nava, A. Castaldini, A. Cavallini, P. Errani, V. Cindro, Radiation Detection Properties of 4H-SiC Schottky Diodes Irradiated Up to 10^{16} n/cm^2 by 1 MeV Neutrons, IEEE Trans. Nucl. Sci. 53 (2006) 2977–2982.
[7] P. Kandlakunta, C. Tan, N. Smith, S. Xue, N. Taylor, R.G. Downing, V. Hlinka, L. R. Cao, Silicon carbide detectors for high flux neutron monitoring at near-core locations, Nucl. Instrum. Methods Phys. Res. A 953 (2020).
[8] A.A. Lebedev, V.V. Kozlovski, P.A. Ivanov, M.E. Levinshtein, A.V. Zubov, Impact of High-Energy Electron Irradiation on Surge Currents in 4H-SiC JBS Schottky Diodes, Semiconductors 53 (2019) 1409–1413.
[9] K. Çınar, C. Coşkun, Ş. Aydoğan, H. Asıl, E. Gür, The effect of the electron irradiation on the series resistance of Au/Ni/6H-SiC and Au/Ni/4H-SiC Schottky contacts, Nucl. Instrum. Methods Phys. Res. B 268 (2010) 616–621.
[10] E. Omotoso, W.E. Meyer, P.J.J. van Rensburg, E. Igumbor, S.M. Tunhuma, P.N. M. Ngoepe, H.T. Danga, F.D. Auret, The effects of high-energy proton irradiation on the electrical characteristics of Au/Ni/4H-SiC Schottky barrier diodes, Nucl. Instrum. Methods Phys. Res. B 409 (2017) 241–245.
[11] J. Vobecký, P. Hazdra, V. Záhlava, A. Mihaila, M. Berthou, ON-state characteristics of proton irradiated 4H–SiC Schottky diode: The calibration of model parameters for device simulation, Solid·state Electron. 94 (2014) 32–38.
[12] P. Hazdra, V. Záhlava, J. Vobecký, Point defects in 4H–SiC epilayers introduced by neutron irradiation, Nucl. Instrum. Methods Phys. Res. B 327 (2014) 124–127.
[13] J. Park, B.-G. Park, H. Baek, G.-M. Sun, Electrical characteristics and deep-level transient spectroscopy of a fast-neutron-irradiated 4H–SiC Schottky barrier diode, Nucl. Eng. Technol. 55 (2023) 201–208.
[14] J.W. Kleppinger, S.K. Chaudhuri, O. Karadavut, R. Nag, D.L.P. Watson, D. S. McGregor, K.C. Mandal, Deep-Level Transient Spectroscopy and Radiation Detection Performance Studies on Neutron Irradiated 250-μm-Thick 4H-SiC Epitaxial Layers, IEEE Trans. Nucl. Sci. 69 (2022) 1972–1978.
[15] T. Brodar, I. Capan, V. Radulović, L. Snoj, Ž. Pastuović, J. Coutinho, T. Ohshima, Laplace DLTS study of deep defects created in neutron-irradiated n-type 4H-SiC, Nucl. Instrum. Methods Phys. Res. B 437 (2018) 27–31.
[16] E. Omotoso, W.E. Meyer, F.D. Auret, A.T. Paradzah, M.J. Legodi, Electrical characterization of deep levels created by bombarding nitrogen-doped 4H-SiC with

alpha-particle irradiation, Nucl. Instrum. Methods Phys. Res. B 371 (2016) 312–316.
[17] L. Zhao, Y. Tang, Y. Bai, M. Qiu, Z. Wu, Y. Yang, C. Yang, X. Tian, X. Liu, Analysis of Defects and Electrical Characteristics of Variable-Temperature Proton-Irradiated 4H-SiC JBS Diodes, Electronics 11 (2022).
[18] I. Capan, T. Brodar, Y. Yamazaki, Y. Oki, T. Ohshima, Y. Chiba, Y. Hijikata, L. Snoj, V. Radulović, Influence of neutron radiation on majority and minority carrier traps in n-type 4H-SiC, Nucl. Instrum. Methods Phys. Res. B 478 (2020) 224–228.
[19] W.J. Zheng C, Li J, et al, Neutron spectra and fluence of CFBR-II reactor measured by foils activation technique, Nucl. Power Eng., 25(1) (2004) 93-96.
[20] D.M.C.R.E. Thomas, Carrier mobilities in silicon empirically related to doping and field, Proc. IEEE 55 (1967) 2192–2193.
[21] W. Shockley, W.T. Read, Statistics of the Recombinations of Holes and Electrons, Phys. Rev. 87 (1952) 835–842.
[22] R.N. Hall, Electron-Hole Recombination in Germanium, Phys. Rev. 87 (1952) 387.
[23] J. Dziewior, W. Schmid, Auger coefficients for highly doped and highly excited silicon, Appl. Phys. Lett. 31 (1977) 346–348.
[24] MeiKei Ieong, P.M. Solomon, S.E. Laux, H.-S.P. Wong, D. Chidambarrao, Comparison of Raised and Schottky Source_Drain MOSFETs Using a Novel Tunneling Contact Model, International Electron Devices Meeting (1998).
[25] K.M.K.U.A. Nishiyama, A unified simulation of Schottky and ohmic contacts, IEEE Trans. Electron Devices, 47 103 - 108.
[26] H.D.M.R. Van Overstraeten, Measurement of the ionization rates in diffused silicon pn junctions, Solid·state Electron. 13 (1970) 583–608.
[27] G.A.M. Hurkx, D.B.M. Klaassen, M.P.G. Knuvers, A New Recombination Model for Device Simulation Including Tunneling, IEEE Trans. Electron Devices 39 (1992).
[28] J.G. Simmons, G.W. Taylor, Nonequilibrium Steady-State Statistics and Associated Effects for Insulators and Semiconductors Containing an Arbitrary Distribution of Traps, Phys. Rev. B 4 (1971) 502–511.
[29] P. Hazdra, V. Zahlava, J. Vobecký, Point defects in 4H–SiC epilayers introduced by neutron irradiation, Nucl. Instrum. Meth. Phys. Res. Sect. B: Beam Interact. Mater. Atoms 327 (2014) 124–127.
[30] J. Vobecky, P. Hazdra, S. Popelka, R.K. Sharma, Impact of Electron Irradiation on the ON-State Characteristics of a 4H–SiC JBS Diode, IEEE Trans. Electron Devices 62 (2015) 1964–1969.
[31] M.R.F. Schwierz, Electron mobility models for 4H, 6H, and 3C SiC [MESFETs], IEEE Trans. Electron Dev. 48 (2001).
[32] M. Boccarossa, A. Borghese, L. Maresca, M. Riccio, G. Breglio, A. Irace, Numerical Analysis of the Schottky Contact Properties on the Forward Conduction of MPS/JBS SiC Diodes, Key Eng. Mater. 947 (2023) 95–102.
[33] S. Wang, R. Hu, G. Chen, C. Luo, M. Gong, Y. Li, M. Huang, Y. Ma, Z. Yang, Investigation of 4H-SiC Schottky barrier diodes irradiated with 6 MeV Au ions at low temperature, Nucl. Instrum. Methods Phys. Res. B 494–495 (2021) 53–58.
[34] S.K. Gupta, N. Pradhan, C. Shekhar, J. Akhtar, Design, Fabrication, and Characterization of Ni/4H-SiC (0001) Schottky Diodes Array Equipped With Field Plate and Floating Guard Ring Edge Termination Structures, IEEE Trans. Semicond. Manuf. 25 (2012) 664–672.
[35] G. Alfieri, E.V. Monakhov, B.G. Svensson, A. Hallén, Defect energy levels in hydrogen-implanted and electron-irradiated n-type 4H silicon carbide, J. Appl. Phys. 98 (2005).
[36] I. Capan, T. Brodar, T. Makino, V. Radulovic, L. Snoj, M-Center in Neutron-Irradiated 4H-SiC, Crystals 11 (2021).
[37] I. Capan, T. Brodar, J. Coutinho, T. Ohshima, V.P. Markevich, A.R. Peaker, Acceptor levels of the carbon vacancy in 4H-SiC: Combining Laplace deep level transient spectroscopy with density functional modeling, J. Appl. Phys. 124 (2018).
[38] B.M.E. Karsthof R, A. Galeckas, et al., Conversion pathways of primary defects by annealing in proton-irradiated n-type 4H-SiC, Phy. Rev. B 102 (18) (2020).
[39] T. Knežević, T. Brodar, V. Radulović, L. Snoj, T. Makino, I. Capan, Distinguishing the EH1 and S1 defects in n-type 4H-SiC by Laplace DLTS, Appl. Phys. Express 15 (2022).